Copperwheat, CM, Morales-Rueda, L, Marsh, TR, Maxted, PFL and Heber, U

 Radial-velocity measurements of subdwarf B stars

http://researchonline.ljmu.ac.uk/id/eprint/5364/

Article

For more information please contact researchonline@ljmu.ac.uk

Radial-velocity measurements of subdwarf B stars

C. M. Copperwheat,[1][*] L. Morales-Rueda,[2] T. R. Marsh,[1] P. F. L. Maxted[3] and U. Heber[4]

[1]*Department of Physics, University of Warwick, Coventry CV4 7AL*
[2]*Symetrica Security Ltd., Phi House, Southampton Science Park, Southampton SO16 7NS*
[3]*Astrophysics Group, Keele University, Keele, Staffordshire ST5 5BG*
[4]*Dr Remeis-Sternwarte, Astronomisches Institut der Universität Erlangen-Nürnberg, Sternwartstr. 7, 96049 Bamberg, Germany*

ABSTRACT

Subdwarf B (sdB) stars are hot, subluminous stars which are thought to be core-helium burning with thin hydrogen envelopes. The mechanism by which these stars lose their envelopes has been controversial, but it has been argued that binary star interaction is the main cause. Over the past decade we have conducted a radial-velocity study of a large sample of sdB stars, and have shown that a significant fraction of the field sdB population exists in binary systems. In 2002 and 2003, we published 23 new binary sdB stars and the definitions of their orbits. Here, we present the continuation of this project. We give the binary parameters for 28 systems, 18 of which are new. We also present our radial-velocity measurements of a further 108 sdBs. Of these, 88 show no significant evidence of orbital motion. The remaining 20 do show radial-velocity variations, and so are good candidates for further study. Based on these results, our best estimate for the binary fraction in the sdB population is 46–56 per cent. This is a lower bound since the radial-velocity variations of very long period systems would be difficult to detect over the baseline of our programme, and for some sources we have only a small number of measurements.

Key words: binaries: close – binaries: spectroscopic – subdwarfs.

1 INTRODUCTION

Subdwarf B stars (sdBs) are hot ($T_{\rm eff} = 25\,000$–$40\,000$ K), core-helium-burning stars with masses $\sim$0.5 M$_\odot$ and thin hydrogen envelopes of mass $\leq$0.02 M$_\odot$ (Heber et al. 1984; Saffer et al. 1994; see also Heber 2009 for a recent review). D'Cruz et al. (1996) proposed that such a star could form if a red giant star with a degenerate helium core were to lose its envelope when it is within $\sim$0.4 mag of the tip of the red giant branch. In this scenario, the core could go on to ignite helium despite the mass-loss. This model explains the masses of sdB stars as a consequence of the core mass at the helium flash.

The loss of the hydrogen envelope could be due to an enhancement of the stellar wind or binary interactions. It has been shown that a large fraction of sdB stars are now members of short-period binary systems (Maxted et al. 2001; Napiwotzki et al. 2004). Close binary systems such as these imply a 'common-envelope' phase, which occurs due to dynamically unstable transfer when the more massive star reaches the red giant phase of its evolution. Orbital energy is then lost to friction, resulting in a shortening of the binary period (Iben & Livio 1993). The common envelope is eventually ejected, leading to an sdB primary star with a close main-sequence

or white dwarf companion (Han et al. 2002, 2003). Yungelson & Tutukov (2005) argued that all sdB stars come from binaries, with the apparently single examples of either the product of merging pairs of helium white dwarfs or members of long-period systems which have avoided the common-envelope phase (Green, Liebert & Saffer 2001), and whose radial-velocity variations we have yet to detect.

SdB stars are of interest because they are a strong test of population synthesis models, since they are much less influenced by the selection effects which compromise other close binary populations, such as cataclysmic variables (Pretorius, Knigge & Kolb 2007). They are also an ideal population for testing models of the common-envelope phase, and sdBs with massive white dwarf companions are one of the potential progenitors for Type Ia supernovae (Tutukov & Yungelson 1981; Webbink 1984).

Following the detection of many close binary sdBs by Maxted et al. (2001), we began a project with the aim of measuring the orbits of a large number of binary systems. In Maxted et al. (2002) and Morales-Rueda et al. (2003b) we published the parameters of 23 systems. We present here the continuation of this study.

2 OBSERVATIONS AND REDUCTION

A complete journal of our observations is given in Table 1. The numbers of radial-velocity observations which we list in this

[*]E-mail: c.copperwheat@warwick.ac.uk

Table 1. Journal of observations.

Dates	No. of radial-velocity (RV) observations	Set-up
2000 April 10–21	18	INT + IDS + 500 mm + R1200R + λ_c = Hα
2001 March 8–13	72	INT + IDS + 500 mm + R1200R + λ_c = Hα
2001 May 1–8	104	INT + IDS + 500 mm + R1200R + λ_c = Hα
2001 August 6–11	76	INT + IDS + 500 mm + R1200B + λ_c = 4350 Å
2001 September 27–October 6	135	INT + IDS + 500 mm + R1200B + λ_c = 4350 Å
2002 March 27–April 1	175	INT + IDS + 500 mm + R1200B + λ_c = 4350 Å
2002 April 23–30	217	INT + IDS + 500 mm + R1200B + λ_c = 4350 Å
2003 March 21–22	35	SAAO 1.9 m + grating spectrograph + grating 4 + λ_c = 4600 Å
2003 April 9–18	101	INT + IDS + 500 mm + R1200B + λ_c = 4400 Å
2003 September 10–15	136	SAAO 1.9 m + grating spectrograph + grating 4 + λ_c = 4600 Å
2004 March 30–April 7	75	SAAO 1.9 m + grating spectrograph + grating 4 + λ_c = 4600 Å
2004 October 22–25	107	SAAO 1.9m + grating spectrograph + grating 4 + λ_c = 4600 Å
2005 June 22–27	101	SAAO 1.9 m + grating spectrograph + grating 4 + λ_c = 4600 Å
2005 October 11–24	223	SAAO 1.9 m + grating spectrograph + grating 4 + λ_c = 4600 Å
2007 March 25–April 6	243	INT + IDS + 500 mm + R1200B + λ_c = 4500 Å
2007 August 17–25	150	INT + IDS + 500 mm + R1200B + λ_c = 4500 Å
2008 March 18–27	61	INT + IDS + 500 mm + R1200B + λ_c = 4500 Å
2009 March 10–16	82	INT + IDS + 500 mm + R1200B + λ_c = 4500 Å
2009 April 30–May 1	12	WHT + ISIS + R600B (λ_c = 4350 Å) + R1200R (λ_c = Hα)

table are those which are presented in this paper, in addition to the measurements previously presented in Maxted et al. (2002) and Morales-Rueda et al. (2003b).

The majority of the data used in this study were collected using the Intermediate Dispersion Spectrograph (IDS) mounted on the 2.5 m Isaac Newton Telescope (INT). Our earliest observations in 2000/2001 used the 500-mm camera with the R1200R grating centred on Hα and the TEK (1k × 1k) CCD giving a dispersion of 0.37 Å pixel^{-1} and a resolution of 0.9 Å. Subsequent observations used the 235-mm camera with the R1200B grating and the thinned EEV10 (2k × 4k) CCD, giving a dispersion of 0.48 Å pixel^{-1} and a resolution of 1.4 Å. The central wavelength used with this grating varied slightly between observing runs, but in all cases was chosen to cover Hβ and Hγ. In 2003, we expanded this project to cover southern targets with the first of a series of observing runs using the grating spectrograph plus the SITe CCD mounted on the 1.9-m telescope at the Sutherland site of the South African Astronomical Observatory (SAAO). Grating 4, with 1200 grooves mm^{-1}, was used to obtain spectra covering Hγ and Hβ with a dispersion of 0.5 Å pixel^{-1} and a resolution of better than 1 Å at 4600 Å.

We took two consecutive observations of each object and bracketed them with CuAr frames to calibrate the spectra in wavelength. After debiasing and flat-fielding the frames (using Tungsten flat-field frames for the INT/IDS observations and dome flats for the SAAO observations), spectral extraction proceeded according to the optimal algorithm of Marsh (1989). The arcs were extracted using the profile associated with their corresponding target to avoid systematic errors caused by the spectra being tilted. Uncertainties on every point were propagated through every stage of the data reduction.

3 RESULTS

3.1 Radial-velocity measurements

To measure the radial velocities, we use least-squares fitting of a model line profile and follow the same procedure described in Morales-Rueda et al. (2003b). The model line profile consists of three Gaussians with different widths and depths. For any given

sdB, the widths and depths of the Gaussians are optimized and then fixed while their velocity offsets from the rest wavelengths of the lines in question are fitted separately for each spectrum; see Maxted, Marsh & Moran (2000) for further details of this procedure. For the red spectra obtained in 2000 April–2001 May we fit the Hα line. For all other spectra the fitting was performed simultaneously for Hβ and Hγ.

In Tables 2 and 3 we list all of our radial-velocity measurements. Table 2 contains the measurements for 28 systems which we have found to be binary, and for which we have found the orbital period. The description of the orbital period determination is given in Section 3.2. Table 3 contains measurements for all of the remaining sdBs covered by our project which we have not previously published, a total of 108 objects. Most of these objects show no evidence for orbital variations, and so are likely to be either single sdBs, or binary systems in which the mass function is too low for us to detect radial-velocity variations (due to a low companion mass, a long binary period, a binary inclination close to zero or a combination of these factors). For some objects the non-detection of variation may be because the number of observations of that object is small. In some other cases, there are clear signs that the sdB is in a binary system; however, there are still competing orbital aliases of comparable significance and so our data are insufficient to determine the true orbital period. These are strong candidates for future observation. In this paper we will concentrate on the 28 solved systems given in Table 2. In Section 4.3 we discuss the binary fraction of the sdB population, and in Section 4.4 we investigate the nature of the companion stars. For these sections we consider the complete list of objects in our programme.

3.2 Determination of orbital periods

In radial-velocity work, while one can very soon determine a star to be binary, it can take much longer to determine the orbital period. With a small amount of data there is a danger of picking an incorrect alias. This period can be very wrong, even when the quoted uncertainty is tiny, because the statistics are not Gaussian and so an error of 100 or even 1000 times the quoted uncertainty can occur. On the other hand, the process of collecting sufficient data to determine

Table 2. Radial-velocity (RV) measurements for the 28 sdB binaries which we present in this paper.

HMJD	RV (km s^{-1})	HMJD	RV (km s^{-1})	HMJD	RV (km s^{-1})	HMJD	RV (km s^{-1})
EC00404−4429		*PG0919+273*		*PG1000+408*		*PG1244+113*	
52892.9858	−124.51 ± 5.13	54902.9529	−74.14 ± 1.26	54191.9382	28.74 ± 2.11	51654.1003	−21.09 ± 5.70
52893.0000	−78.05 ± 5.11	54902.9704	−74.38 ± 1.26	54191.9522	33.23 ± 2.00	51977.1722	−32.37 ± 9.29
52893.1529	96.73 ± 4.86	*PG0934+186*		*PG1230+052*		51977.1827	−48.06 ± 9.30
52893.1671	161.87 ± 5.97	52360.9826	67.29 ± 3.19	52387.9376	−85.66 ± 11.24	51982.1343	−20.65 ± 6.05
52893.9884	−28.82 ± 4.12	52360.9966	70.62 ± 3.21	52387.9534	−78.37 ± 8.46	51982.1448	−17.57 ± 5.95
52894.0041	−113.13 ± 4.23	52361.0510	66.46 ± 2.65	52390.9528	−7.95 ± 2.09	51982.2290	−11.29 ± 7.18
52894.0197	−106.96 ± 4.23	52361.0650	67.23 ± 2.58	52390.9635	−8.77 ± 2.87	51982.2394	−10.75 ± 7.49
52896.9267	58.39 ± 5.80	52361.9272	3.88 ± 3.17	52390.9973	−12.45 ± 3.94	52030.9039	54.66 ± 10.34
52896.9409	−32.49 ± 5.36	52361.9343	3.64 ± 2.95	52391.0045	−11.92 ± 3.54	52030.9144	34.65 ± 10.91
EC02200−2338		52361.9683	4.40 ± 2.86	52391.8989	−20.38 ± 1.83	52032.0570	60.34 ± 4.50
52893.0509	−28.99 ± 2.08	52361.9754	5.34 ± 2.82	52391.9096	−30.06 ± 1.94	52032.0726	53.38 ± 6.78
52893.0617	−24.97 ± 2.10	52362.0590	−15.04 ± 3.03	52391.9831	−52.42 ± 2.16	52036.0392	−8.67 ± 13.21
52894.0688	107.97 ± 1.75	52362.0661	−11.18 ± 3.39	52391.9903	−56.15 ± 2.12	52036.0545	3.31 ± 7.99
52894.0795	110.91 ± 1.81	52387.8990	−27.67 ± 9.85	52392.1596	−88.17 ± 9.54	52036.0693	8.56 ± 5.67
52896.9574	−72.84 ± 2.39	52387.9096	−24.38 ± 8.36	52393.1168	−72.13 ± 3.98	52037.0903	58.40 ± 8.37
52896.9680	−73.29 ± 2.41	52389.9387	31.38 ± 8.96	52393.1240	−72.62 ± 3.94	52037.1007	68.93 ± 9.54
52897.1604	41.92 ± 2.34	52389.9494	31.72 ± 9.73	52394.0944	−25.06 ± 2.23	52037.9680	58.30 ± 15.66
52897.1710	47.89 ± 3.26	52391.9454	−20.38 ± 2.26	52394.1016	−26.25 ± 2.26	52038.0319	38.46 ± 8.41
52897.9449	30.21 ± 2.64	52391.9561	−20.29 ± 2.04	52394.9025	−35.08 ± 2.56	52038.0681	66.28 ± 9.72
52897.9570	33.80 ± 2.41	52392.8678	53.23 ± 2.88	52394.9097	−36.52 ± 2.49	52390.9009	−44.48 ± 3.58
PG0919+273		52392.8750	51.52 ± 2.93	54186.1483	−67.97 ± 5.52	52390.9150	−44.56 ± 3.26
51652.8518	−77.20 ± 4.07	*PG0958−073*		54186.1589	−74.42 ± 4.93	52391.0531	−38.86 ± 6.66
51652.8562	−83.25 ± 3.84	52362.8649	97.72 ± 4.05	54188.9017	−45.82 ± 3.72	52391.0672	−59.23 ± 7.39
51653.9461	−57.47 ± 3.21	52362.8766	107.06 ± 4.10	54188.9122	−63.98 ± 2.45	52392.9466	19.61 ± 5.07
51653.9505	−58.29 ± 3.15	52363.8644	107.47 ± 4.95	54190.0697	−9.41 ± 2.04	52392.9538	15.33 ± 4.91
52361.8796	−51.08 ± 3.74	52363.8762	106.10 ± 4.62	54190.0803	−8.91 ± 1.90	54185.1282	−19.35 ± 4.23
52361.8832	−59.99 ± 3.22	54189.9787	102.64 ± 2.01	54191.0239	−37.35 ± 2.17	54185.1422	−22.98 ± 3.98
52361.9143	−54.96 ± 3.57	54189.9928	97.55 ± 2.05	54191.0344	−40.40 ± 2.39	54187.9900	29.69 ± 7.38
52361.9179	−51.01 ± 3.56	54544.9753	102.47 ± 2.62	*EC12408−1427*		54188.0040	33.74 ± 2.91
52364.8420	−90.86 ± 5.55	54544.9894	103.73 ± 2.34	52359.9674	8.30 ± 5.73	54191.0610	−44.49 ± 4.35
52364.8491	−91.81 ± 4.45	54546.9353	68.73 ± 3.49	52359.9791	0.21 ± 5.97	54191.0802	−36.60 ± 2.28
52387.8743	−39.18 ± 4.36	54546.9529	58.76 ± 2.68	52363.9527	−90.29 ± 4.04	54196.0172	6.74 ± 2.57
52387.8850	−43.35 ± 3.89	54903.9622	72.19 ± 1.83	52363.9633	−98.45 ± 4.34	54196.0381	9.68 ± 2.50
52389.8909	−30.85 ± 2.62	54903.9762	71.23 ± 1.74	52364.0110	−113.52 ± 5.07	54197.0684	−43.90 ± 3.41
52389.8981	−26.64 ± 2.70	54905.9308	74.35 ± 1.60	52364.0217	−115.04 ± 5.64	54197.0859	−48.21 ± 2.77
52391.9656	−34.87 ± 2.84	54905.9518	82.43 ± 1.66	52364.9004	−110.89 ± 2.71	54544.1241	−2.47 ± 2.89
54184.8900	−51.89 ± 2.11	54906.0913	83.40 ± 2.13	52364.9099	−107.96 ± 2.79	54544.1381	14.10 ± 2.83
54184.9006	−53.22 ± 2.17	54906.1106	79.36 ± 2.55	52364.9700	−104.87 ± 3.02	54901.0952	26.49 ± 10.20
54185.8630	−71.15 ± 2.81	54906.9068	70.36 ± 0.81	52364.9783	−109.31 ± 3.17	54901.1162	6.13 ± 10.76
54185.9145	−69.80 ± 2.37	54906.9278	71.31 ± 2.31	52365.1026	−83.42 ± 6.50	54901.1607	30.62 ± 9.24
54186.9793	−91.95 ± 2.41	54906.9976	71.11 ± 1.90	52365.1109	−79.30 ± 5.76	54904.0400	−15.81 ± 3.78
54186.9898	−84.68 ± 2.54	54907.0185	74.90 ± 2.57	52719.0414	−11.55 ± 3.49	54904.0610	−13.37 ± 7.22
54188.9296	−106.43 ± 1.49	54907.0419	71.59 ± 2.06	52719.0520	−9.66 ± 3.53	54904.0843	−8.45 ± 6.61
54188.9401	−109.01 ± 1.50	*PG1000+408*		52720.0622	7.57 ± 5.20	54906.1353	−4.33 ± 3.77
54189.8946	−113.90 ± 1.71	51648.8644	80.31 ± 16.63	52720.0728	8.58 ± 5.38	54906.1494	−3.53 ± 3.78
54189.9051	−108.21 ± 1.75	51648.8687	79.03 ± 13.64	53095.8583	−117.18 ± 6.85	54951.9511	−21.41 ± 1.94
54192.9248	−84.69 ± 1.44	51650.8991	101.74 ± 6.12	53095.8797	−109.81 ± 10.61	54951.9651	−21.32 ± 1.90
54192.9353	−80.55 ± 1.38	51650.9054	101.82 ± 5.91	53101.0041	40.10 ± 51.44	54951.9778	−15.29 ± 2.58
54196.8596	−30.57 ± 1.71	51650.9197	92.60 ± 6.46	53101.0148	−47.01 ± 55.80	*PG1253+284*	
54196.8702	−29.34 ± 1.69	51650.9260	91.82 ± 6.27	53101.9736	−21.44 ± 14.52	52393.8556	−7.91 ± 2.85
54900.8833	−42.30 ± 1.51	51655.8593	78.81 ± 7.08	53101.9843	−49.64 ± 15.96	52393.8628	−4.66 ± 2.21
54900.9043	−35.82 ± 2.30	51655.8661	112.09 ± 7.10	53102.9589	−70.09 ± 2.67	52394.0000	−1.98 ± 1.21
54900.9271	−45.03 ± 1.81	51656.8492	70.89 ± 6.34	53102.9800	−71.58 ± 4.17	52394.0106	−5.39 ± 1.27
54900.9481	−46.61 ± 2.35	51656.8575	84.64 ± 5.46	53546.7334	28.67 ± 32.01	52394.9430	22.07 ± 1.16
54901.0388	−41.93 ± 3.19	54185.9322	114.52 ± 3.13	53546.7490	−15.70 ± 11.63	52394.9571	23.00 ± 1.15
54901.0597	−36.78 ± 3.16	54185.9462	117.23 ± 2.62	53546.7664	−19.69 ± 26.73	54186.1194	−7.66 ± 3.73
54901.8701	−57.47 ± 2.58	54188.0181	117.70 ± 1.97	53548.7051	−50.43 ± 5.21	54186.1789	−6.99 ± 7.96
54901.8911	−56.96 ± 1.74	54188.0321	119.15 ± 2.15	53548.7196	−52.11 ± 5.07	54188.1001	16.52 ± 1.12
54901.9788	−55.82 ± 2.36	54188.8607	56.51 ± 3.41	*PG1244+113*		54188.1141	17.55 ± 1.10
54901.9998	−59.26 ± 2.15	54188.8747	59.13 ± 2.54	51646.0409	65.12 ± 5.56	54189.0028	−3.40 ± 0.95
54902.0231	−51.54 ± 2.65	54189.8591	36.54 ± 2.22	51646.0505	68.70 ± 5.79	54189.0168	−3.73 ± 0.91
54902.0441	−50.07 ± 2.65	54189.8732	44.35 ± 2.24	51654.0907	−13.70 ± 6.66	54190.1043	44.29 ± 1.09

Table 2. – *continued*

HMJD	RV (km s^{-1})	HMJD	RV (km s^{-1})	HMJD	RV (km s^{-1})	HMJD	RV (km s^{-1})
PG1253+284		*PG1439−013*		*PG1519+640*		*PG1558−007*	
54190.1183	43.52 ± 1.08	52360.0982	−109.88 ± 15.03	52390.9823	38.86 ± 2.47	53103.0441	−99.63 ± 2.87
54191.1132	15.61 ± 0.85	52363.0472	−5.19 ± 9.27	52391.0106	35.96 ± 4.38	53103.0651	−101.28 ± 2.96
54191.1255	17.70 ± 1.00	52363.0578	−14.69 ± 10.56	52391.0143	35.17 ± 5.33	53543.9387	−60.22 ± 8.61
54193.9361	18.93 ± 0.91	52719.9969	−28.05 ± 12.92	52391.0180	30.89 ± 5.72	53543.9531	−51.02 ± 9.63
54193.9501	19.01 ± 0.91	52720.0110	1.88 ± 13.70	52391.0217	34.95 ± 4.61	53544.8236	−88.18 ± 6.64
54195.0801	−2.82 ± 1.17	52721.1381	−40.15 ± 15.78	52391.1023	11.34 ± 2.82	53544.8377	−91.40 ± 6.35
54195.0941	−2.57 ± 1.21	52721.1555	−29.99 ± 17.16	52391.1129	12.92 ± 2.43	54185.2330	−59.72 ± 1.83
54544.2634	8.98 ± 1.09	54187.2025	−30.06 ± 4.24	52391.1236	−2.39 ± 2.30	54185.2561	−56.59 ± 2.57
54544.2774	6.86 ± 1.37	54187.2130	−36.47 ± 6.69	52391.2178	−35.83 ± 1.72	54188.2227	−112.46 ± 1.86
54553.0913	17.50 ± 3.32	54188.1291	−77.06 ± 3.91	52391.2285	−36.85 ± 1.77	54188.2368	−123.80 ± 1.85
54553.1054	5.45 ± 4.06	54188.1397	−77.72 ± 3.85	52392.0016	24.74 ± 1.95	*PG1648+536*	
54553.1217	4.33 ± 4.66	54189.1089	−99.58 ± 3.88	52392.0088	31.94 ± 1.69	52394.1708	−79.50 ± 2.16
54553.1358	13.39 ± 6.35	54189.1195	−95.59 ± 4.03	52392.2246	−16.38 ± 3.67	52394.1850	−64.36 ± 2.15
54904.1128	1.30 ± 2.53	54190.1324	−90.95 ± 3.31	52392.2283	−15.59 ± 3.78	52394.9886	21.58 ± 3.64
54904.1268	0.88 ± 1.42	54190.1430	−96.19 ± 3.34	*PG1528+104*		52394.9993	15.69 ± 3.30
54904.1555	3.89 ± 1.00	54194.0632	−14.17 ± 2.96	52394.0261	−21.63 ± 2.14	52395.0745	−49.68 ± 3.59
54904.1695	4.61 ± 0.99	54194.0738	−16.21 ± 3.12	52394.0368	−32.06 ± 2.16	52395.0852	−67.88 ± 3.36
54951.9998	−12.82 ± 0.54	54194.1785	−25.47 ± 3.35	52394.1208	−96.93 ± 2.58	52395.1288	−107.80 ± 3.00
54952.0127	−6.84 ± 0.64	54194.1890	−25.31 ± 3.44	52394.1280	−99.33 ± 2.57	52395.1395	−124.28 ± 3.48
EC13332−1424		54194.9956	−45.77 ± 3.93	52394.2024	−73.71 ± 2.50	52395.1722	−145.89 ± 4.09
52363.0216	−155.91 ± 6.04	54195.0062	−44.86 ± 3.68	52394.2096	−65.22 ± 2.49	52395.1829	−143.67 ± 4.16
52363.0323	−152.81 ± 5.70	54195.1788	−70.63 ± 3.09	52394.2355	−27.17 ± 4.89	52395.1948	−161.91 ± 4.21
52365.0258	18.54 ± 3.49	54195.1975	−63.45 ± 3.19	52394.2385	−21.96 ± 5.20	54189.1981	45.25 ± 1.70
52365.0399	22.39 ± 3.47	54196.0543	−99.24 ± 2.85	52394.2444	−20.56 ± 5.81	54189.2156	38.45 ± 2.32
52365.0767	44.76 ± 5.03	54196.0683	−97.67 ± 2.94	52394.2474	−23.83 ± 6.70	54194.0212	22.88 ± 1.96
52365.0884	52.69 ± 5.82	54544.1851	−26.81 ± 3.08	52394.9724	2.72 ± 3.08	54194.0422	29.17 ± 1.83
52719.0138	−145.30 ± 5.81	54544.1991	−24.84 ± 3.21	52394.9796	3.16 ± 3.19	54905.2272	23.34 ± 2.35
52719.0244	−138.72 ± 5.43	54545.2409	−65.42 ± 3.76	52395.0579	−56.44 ± 3.59	54905.2481	10.15 ± 1.88
52720.1602	−21.03 ± 14.31	54545.2550	−74.41 ± 2.90	52395.0651	−66.74 ± 3.33	54906.2541	−51.00 ± 3.81
52720.1709	−32.34 ± 21.87	54545.2746	−77.45 ± 5.14	*PG1558−007*		54906.2699	−37.40 ± 4.74
53095.9061	−100.89 ± 11.02	54901.1879	3.93 ± 10.56	52363.0998	−53.35 ± 4.77	54907.1534	−64.02 ± 2.84
53095.9272	−117.66 ± 22.13	54901.2089	−25.17 ± 10.10	52363.1139	−42.38 ± 5.08	54907.1709	−85.85 ± 2.86
53099.9697	−166.82 ± 9.09	54902.1478	−48.62 ± 4.57	52365.1246	−91.64 ± 4.52	*KUV16256+4034*	
53099.9839	−152.39 ± 6.60	54902.1722	−44.25 ± 4.30	52365.1364	−95.26 ± 4.80	52390.0852	−100.88 ± 1.81
53102.0324	45.80 ± 7.99	54902.1976	−52.51 ± 4.38	52365.1493	−116.79 ± 5.67	52390.1063	−92.64 ± 1.32
53102.0535	28.58 ± 9.74	54902.2186	−48.68 ± 3.98	52720.1184	−94.85 ± 9.57	52391.0316	−104.73 ± 3.20
53103.0057	−30.37 ± 5.38	*PG1452+198*		52720.1325	−100.38 ± 9.97	52391.0370	−117.84 ± 3.41
53103.0268	−51.83 ± 4.61	52129.8666	−85.36 ± 1.60	52740.0952	−106.39 ± 2.62	52391.1596	−55.83 ± 1.85
53544.7500	−45.95 ± 14.60	52129.8736	−84.52 ± 1.61	52740.1059	−104.39 ± 2.61	52391.1703	−50.52 ± 1.72
53544.7642	−36.59 ± 16.27	52130.8653	−77.72 ± 2.36	52743.1068	−40.45 ± 6.52	52392.0236	−91.67 ± 1.22
53545.8428	42.44 ± 10.02	52130.8730	−75.80 ± 2.39	52744.0989	−28.24 ± 4.19	52392.0342	−87.38 ± 1.31
53545.8569	27.77 ± 10.80	52363.2145	−70.30 ± 6.48	52744.1084	−37.38 ± 4.60	52392.2046	−67.39 ± 1.41
PG1403+316		52363.2183	−81.25 ± 6.24	52744.1535	−34.79 ± 3.31	52392.2153	−74.06 ± 1.38
52393.8996	36.24 ± 3.71	52387.9709	88.75 ± 9.54	52744.1653	−29.95 ± 3.24	52392.9629	−96.40 ± 2.12
52393.9068	34.68 ± 3.39	52387.9816	75.69 ± 5.36	52745.0541	−25.33 ± 3.01	52392.9701	−89.53 ± 2.02
52395.0143	5.30 ± 2.78	52388.0467	53.95 ± 3.41	52745.0647	−28.71 ± 2.79	52393.0702	−49.53 ± 1.71
52395.0215	−1.45 ± 2.62	52388.0608	41.67 ± 2.98	52745.1642	−33.13 ± 2.27	52393.0774	−50.74 ± 1.70
52395.1003	18.09 ± 3.20	52389.9907	47.50 ± 3.96	52745.1760	−35.09 ± 2.30	52394.2178	−110.64 ± 1.30
52395.1075	22.83 ± 3.45	52389.9979	40.25 ± 4.29	52745.2281	−30.03 ± 2.70	52394.2250	−117.45 ± 1.35
52395.1547	26.11 ± 3.74	52390.0596	15.29 ± 3.46	52747.0890	−65.50 ± 3.13	52395.2201	−127.88 ± 1.96
52395.1619	30.42 ± 3.65	52390.0668	5.10 ± 4.61	52747.1013	−64.13 ± 2.55	52395.2273	−127.28 ± 2.10
54187.1596	−39.00 ± 1.94	52390.9380	55.73 ± 3.21	52747.1176	−67.88 ± 3.15	*EC20182−6534*	
54187.1806	−36.08 ± 2.06	52390.9417	53.66 ± 3.16	52747.1282	−65.71 ± 3.39	52896.8455	35.31 ± 5.78
54193.9656	−58.24 ± 1.46	52392.0960	−34.22 ± 3.75	52746.2195	−39.57 ± 2.36	52896.8561	32.46 ± 5.13
54193.9866	−55.08 ± 1.43	52392.0998	−52.67 ± 2.55	52892.7187	−84.44 ± 3.86	52897.8218	40.52 ± 6.68
54194.2050	−20.80 ± 1.41	52395.2096	−92.54 ± 3.75	52892.7333	−83.42 ± 3.59	52897.8324	44.59 ± 6.77
54194.2260	−13.98 ± 1.78	52395.2133	−94.66 ± 3.70	52893.7168	−113.83 ± 4.22	53301.7904	−14.56 ± 18.41
54194.9545	44.41 ± 1.96	*PG1519+640*		52893.7310	−104.84 ± 3.65	53301.8041	−40.34 ± 10.65
54194.9685	36.62 ± 1.89	52390.1887	−34.63 ± 1.92	52894.7609	−122.43 ± 9.74	53302.7609	76.03 ± 5.85
PG1439−013		52390.2261	−28.40 ± 2.17	52895.7187	−108.77 ± 4.09	53302.7737	80.02 ± 7.25
52360.0700	−125.61 ± 16.96	52390.2367	−22.02 ± 1.93	53095.1184	−45.75 ± 5.32	53303.7586	−1.28 ± 23.51
52360.0841	−109.78 ± 16.13	52390.9751	34.98 ± 2.38	53095.1395	−60.46 ± 6.21	53303.7719	12.97 ± 8.03

Table 2. – *continued*

HMJD	RV (km s^{-1})	HMJD	RV (km s^{-1})	HMJD	RV (km s^{-1})	HMJD	RV (km s^{-1})
EC20182−6534		*EC20369−1804*		*EC21556−5552*		*EC22590−4819*	
53303.8700	68.48 ± 7.28	52893.9340	−6.77 ± 3.96	53655.9307	79.46 ± 6.34	52896.8993	54.81 ± 7.33
53303.8841	64.39 ± 7.20	52895.8477	−7.98 ± 9.60	53655.9414	62.31 ± 6.25	52896.9100	45.90 ± 14.20
53543.9901	49.05 ± 9.75	53300.8000	−40.33 ± 5.98	53656.8616	19.04 ± 5.09	52897.9100	67.73 ± 4.92
53544.0012	75.57 ± 16.40	53300.8108	−43.49 ± 6.39	53656.8723	22.31 ± 4.95	52897.9207	54.27 ± 5.96
53546.0133	11.16 ± 8.18	53301.8784	11.87 ± 5.51	53657.8573	−26.69 ± 6.93	53663.7933	53.59 ± 6.61
53546.0276	3.25 ± 7.47	53301.8891	12.50 ± 6.41	53657.8680	−22.73 ± 7.06	53663.8041	56.54 ± 6.54
53549.0111	−4.07 ± 7.40	53302.8296	53.09 ± 8.23	53658.8801	4.88 ± 12.27	*EC22590−4819*	
53549.0219	4.63 ± 7.17	53302.8403	61.51 ± 7.97	53658.8908	−2.28 ± 14.54	53664.8451	5.01 ± 7.54
53549.1810	−44.75 ± 7.76	53303.7928	18.90 ± 6.53	53659.8115	49.63 ± 6.43	53300.8525	58.12 ± 4.92
53654.8809	49.50 ± 8.83	53303.8035	22.68 ± 6.69	53659.8222	53.49 ± 5.10	53302.9837	45.65 ± 6.79
53654.8919	63.31 ± 11.29	53544.1446	−67.58 ± 23.49	53665.9305	68.31 ± 8.23	53302.9953	47.91 ± 8.37
53655.8991	19.20 ± 8.59	53544.1591	−67.34 ± 23.03	53663.7933	53.59 ± 6.61	53303.9058	19.18 ± 4.67
53655.9102	12.20 ± 8.59	53547.0553	60.74 ± 9.35	53663.8041	56.54 ± 6.54	53303.9165	18.58 ± 4.59
53656.7602	25.21 ± 6.00	53547.0698	40.14 ± 8.39	53664.8451	5.01 ± 7.54	53545.1258	−32.26 ± 4.78
53656.7710	14.87 ± 6.09	53656.8328	−50.54 ± 7.76	53666.9076	16.96 ± 5.67	53545.1365	−32.90 ± 5.41
EC20260−4757		53656.8435	−37.86 ± 8.38	53666.9186	−13.67 ± 5.88	53546.1411	−31.16 ± 10.75
52894.9204	65.63 ± 10.86	53659.8427	50.76 ± 8.39	*KPD2215+5037*		53546.1554	−28.23 ± 5.01
52894.9528	82.99 ± 16.01	53659.8534	44.36 ± 10.80	52183.1287	52.29 ± 2.76	53656.9639	−10.36 ± 10.23
52895.8292	89.89 ± 9.46	53663.7933	53.59 ± 6.61	52183.1357	42.32 ± 2.86	53656.9804	3.87 ± 6.32
52896.7817	114.17 ± 6.33	53663.8041	56.54 ± 6.54	52187.0800	79.97 ± 2.97	53657.9064	−24.32 ± 4.99
52896.7959	111.24 ± 6.78	53664.8451	5.01 ± 7.54	52187.0871	81.66 ± 2.95	53657.9171	−18.33 ± 4.96
52897.7588	90.95 ± 5.85	53664.8558	10.24 ± 7.69	52188.1216	−36.50 ± 2.96	53661.9111	38.85 ± 5.34
52897.7729	87.38 ± 5.96	53665.7515	−43.03 ± 6.44	52188.1287	−42.42 ± 3.10	53661.9254	15.74 ± 5.21
52897.9743	92.70 ± 14.57	*KPD2040+3955*		54330.1392	−82.78 ± 1.95	53666.9366	1.91 ± 6.15
52897.9885	77.23 ± 8.88	52184.0383	−60.06 ± 3.07	54330.1532	−83.14 ± 1.76	53666.9473	1.51 ± 6.29
52898.0010	78.52 ± 13.64	52184.0488	−55.54 ± 4.95	54331.8848	−20.74 ± 1.54	*PG2331+038*	
53300.7559	122.82 ± 9.00	52187.0305	−51.00 ± 3.00	54331.9023	−15.67 ± 1.45	52132.1785	−62.47 ± 4.68
53300.7797	121.78 ± 5.55	52187.0410	−42.91 ± 3.08	54333.1244	−15.83 ± 1.28	52132.1891	−61.35 ± 5.23
53301.8299	56.54 ± 5.09	52187.9203	−33.00 ± 2.53	54333.1419	−15.26 ± 1.36	52133.0754	−71.59 ± 3.43
53301.8526	45.62 ± 4.54	52187.9308	−34.74 ± 2.48	*EC22202−1834*		52133.0895	−77.34 ± 3.41
53302.8625	27.63 ± 6.75	52188.8410	67.40 ± 3.04	53544.1835	−71.66 ± 9.30	52187.1413	−3.65 ± 4.23
53302.8851	9.04 ± 5.16	52188.8515	74.17 ± 3.37	53545.0884	−71.74 ± 10.54	52187.1501	−4.18 ± 5.95
53303.8246	−6.66 ± 6.42	52189.0179	77.28 ± 3.18	53545.1056	−51.14 ± 7.73	54331.1209	−93.39 ± 3.26
53303.8472	−9.59 ± 6.20	52392.1846	80.69 ± 4.94	53546.1041	92.64 ± 8.46	54331.1419	−90.49 ± 4.08
53544.0935	31.44 ± 14.63	52393.1329	−61.16 ± 5.39	53546.1166	80.07 ± 21.73	54332.9926	75.74 ± 4.25
53544.1148	50.75 ± 13.41	52393.1470	−54.23 ± 5.21	53549.2076	−138.46 ± 14.68	54333.0136	62.61 ± 4.28
53546.0572	3.10 ± 4.72	54330.0499	48.10 ± 2.24	53656.9250	−84.10 ± 10.41	54333.1706	2.16 ± 2.61
53546.0785	10.30 ± 6.15	54330.0674	53.93 ± 2.07	53661.9477	−130.65 ± 11.82	54333.1915	−14.80 ± 2.70
53547.0094	28.71 ± 15.17	54331.9681	12.44 ± 3.18	53661.9620	−135.68 ± 13.25	54335.0123	3.08 ± 2.77
53547.0305	28.38 ± 9.84	54331.9856	11.53 ± 3.96	53663.9314	−41.10 ± 5.93	54335.0332	5.68 ± 2.57
53549.0464	101.67 ± 7.43	54332.8663	21.47 ± 9.37	53663.9456	−56.59 ± 6.07	54336.0388	−91.54 ± 2.63
53549.0675	96.19 ± 8.00	54332.8804	14.44 ± 6.10	53666.7486	−37.10 ± 5.84	54336.0597	−82.12 ± 2.84
53656.7914	105.77 ± 9.70	54334.1887	−67.00 ± 2.75	53666.7629	−39.40 ± 6.11	54338.0645	−42.37 ± 3.22
53656.8092	106.18 ± 7.70	54334.2062	−65.34 ± 2.85	53667.8629	64.20 ± 17.35	54338.0854	−46.50 ± 2.89
53658.8182	82.88 ± 5.21	*EC21556−5552*		*EC22590−4819*			
EC20369−1804		53654.9135	98.33 ± 15.59	52893.9488	−12.30 ± 2.65		
52893.9233	−5.02 ± 3.98	53654.9261	109.47 ± 16.25	52893.9595	−15.22 ± 2.69		

the true period beyond doubt can be very inefficient in terms of telescope time. It was therefore necessary for us to select a criterion by which we consider a binary orbit to be solved.

Our initial 'rule of thumb' was to consider the period in a system to be determined if the lowest minimum of the χ^2 function has a χ^2 at least 10 less than the next lowest minimum. From a Bayesian point of view, this $\Delta\chi^2 > 10$ criterion is equivalent to requiring that the second best period is $\gtrsim \exp 5 = 150$ times less probable than the best. This argument, although true, is not precise because while the peak of the second alias may be >150 times less probable than the peak of the best alias, there is no guarantee that the total probability of *any* other period is as low. We therefore instead chose

to determine the probabilities of the true orbital period being within a certain range of our favoured value. The details of this Bayesian calculation are given in Morales-Rueda et al. (2003b) and Marsh, Dhillon & Duck (1995). For the purposes of comparing the observed sdB binary-period distribution to theoretical evolutionary models, knowing the orbital period to within ±5 per cent is sufficient. We therefore established the following criterion: we considered a system to be solved if the probability that the true orbital period lies further than 5 per cent from our best alias is less than 0.1 per cent.

For 28 of our targets we have enough radial-velocity measurements to satisfy this criterion. We have previously announced nine of these in conference proceedings (PG0934+186, PG1230+052,

Table 3. Previously unpublished radial velocities for the remaining sdBs in our survey. Some of these show no significant variation. Others (which we mark with an asterisk) show signs of orbital variations, but our data are insufficient to distinguish between competing aliases. This print version lists measurements for three of the 108 sdBs. The full table is available in the electronic version of this paper (see Supporting Information).

HMJD	RV (km s^{-1})	HMJD	RV (km s^{-1})	HMJD	RV (km s^{-1})	HMJD	RV (km s^{-1})
EC00042−2737		*PG0004+133*		*PG0004+133*		*PG0005+179**	
53303.9894	33.51 ± 9.34	54335.2150	−9.53 ± 1.21	54343.2136	−7.32 ± 1.13	54332.1726	−48.04 ± 5.02
53304.0040	30.00 ± 10.31	54335.2290	−7.76 ± 1.17	54343.2276	−6.09 ± 1.16	54333.0405	−49.54 ± 3.57
53547.1765	39.25 ± 8.63	54337.1654	0.41 ± 1.20	54343.2437	−0.51 ± 1.12	54333.0580	−53.90 ± 3.57
53657.9673	36.81 ± 11.90	54337.1794	−1.81 ± 1.21	*PG0005+179**		54333.2292	−53.70 ± 5.90
53657.9815	45.64 ± 11.38	54342.2151	5.38 ± 1.83	52186.1804	−8.00 ± 5.55	54333.2467	−50.77 ± 8.16
53664.0050	34.68 ± 12.99	54342.2291	1.61 ± 1.40	52186.1926	3.00 ± 6.85	54334.0350	−10.59 ± 3.41
53664.0207	3.85 ± 9.21	54342.2519	3.22 ± 2.59	52188.1516	36.14 ± 3.95	54334.0525	−15.38 ± 3.37
53665.0124	28.70 ± 3.85	54343.0948	−8.68 ± 1.60	52188.1658	28.83 ± 4.07	54342.0056	11.98 ± 6.40
PG0004+133		54343.1089	−1.81 ± 1.26	54331.1744	−3.56 ± 4.02	54342.0231	3.56 ± 3.58
54332.2006	−0.58 ± 1.23	54343.1799	5.24 ± 1.22	54331.1919	−1.06 ± 4.53		
54332.2181	−1.13 ± 1.21	54343.1940	−0.77 ± 1.15	54332.1551	−44.84 ± 5.43		

PG1244+113, PG1519+640, PG1528+104, KPD2040+3955, Morales-Rueda et al. 2003a; EC00404−4429, EC02200−2338, Morales-Rueda et al. 2005; EC12408−1427, Morales-Rueda et al. 2006), but we present here the more detailed analysis. The orbit of one of our targets has been independently determined (PG1000+408; Shimanskii et al. 2008), and so we present our results to corroborate this determination. The remaining 18 orbital determinations are new.

We follow the procedure described in Morales-Rueda et al. (2003b), using the 'floating mean' periodogram (e.g. Cumming, Marcy & Butler 1999), which consists in fitting the data with a model composed of a sinusoid plus a constant of the form

$$V = \gamma + K \sin(2\pi f(t - t_0)),$$

where f is the frequency ($f = 1/\text{period}$) and t is the observation time. We obtain the χ^2 of the fits as a function of frequency and select the minima of this χ^2 function. By fitting the systemic velocity, γ, at the same time as K and t_0, we correct a failing of the Lomb–Scargle (Lomb 1976; Scargle 1982) periodogram which starts by subtracting the mean of the data and then fits a plain sinusoid. The floating mean periodogram works better than the Lomb–Scargle periodogram for small number of points. We obtain the χ^2 of the fit as a function of f and then identify minima in this function.

In Table 4 we give the orbital parameters for each sdB binary, listing T_0, the systemic velocity, γ, the radial-velocity semi-amplitude, K, and the reduced χ^2 achieved for the best alias. We also give the period of an Nth alias, and the difference in χ^2 between this alias and the best alias. In most cases we list the $N = 2$ alias, and find a significant χ^2 difference between these best and second best aliases. However, for some systems (PG0958−073, PG1000+408, PG1230+052, PG1403+316, PG1648+536, KPD2215+5037 and PG2331+038) we find that the best alias is surrounded by many other aliases which are very close in period and with a similar χ^2. In some sense these systems are not solved since these close aliases are as significant as the best alias, but they are sufficiently close and span a sufficiently small range that our criterion is satisfied. For the purposes of Table 4, when the nearest competing aliases are so close in period it makes more sense to compare them with the next *group* of aliases, so for these systems we choose to give the Nth alias for which the period differs by more than 5 per cent from the

best alias. In all cases this results in a significant difference in χ^2 between this alias and the best alias.

The results of folding the radial velocities of each object on its orbital period are plotted in Fig. 1. The error bars on the radial-velocity points are, in most cases, smaller than the size of the symbol used to display them.

The periodograms (χ^2 versus orbital frequency) for the 28 objects listed in Table 4 are given in Figs 2 and 3. Each panel includes a blow-up of the region in frequency where the minimum χ^2 is found. It is clear from these figures that in the majority of cases there is a significant difference in χ^2 between the best alias and the second alias. Exceptions are the seven systems we have previously discussed in which there are many aliases close in frequency and significance to the best alias. The blow-ups illustrate that the frequency range covered by these alternate aliases is very small, so we can determine the period to within 5 per cent of the true value with confidence. Two other systems we wish to highlight are PG1452+198 and EC22202−1834. In Table 4 we compare the first and second aliases for these systems, which are very similar in significance. The periodograms for each of these two systems show that the two aliases are discrete and separate without the continuous range of intermediate aliases which we see in the previously discussed seven systems. For each system, either one of these two solutions could represent the 'true' period, and the χ^2 difference is too small to favour one over the other. However, in both cases the period difference between the two aliases is very small and our criterion for the solution is satisfied no matter which we believe to be the true period. We therefore include these systems with those we consider to be solved.

In Table 5 we list for each system the probability that the true orbital period lies further than 1 and 5 per cent from our favoured value, using the Bayesian calculation detailed in Morales-Rueda et al. (2003b) and Marsh et al. (1995). We consider a period to be robust when the probability is below 0.1 per cent (or −3 in the log scale). This is not fulfilled to within 1 per cent of our favoured period for seven of our 28 sources. The worst example is PG1519+640: for this system the probability that the true period is more than 1 per cent different from our favoured value is −0.98 in the log scale, or greater than 10 per cent. However, all of the periods are robust to within 5 per cent of our favoured values, and as we noted earlier

Table 4. List of the orbital periods measured for the 28 sdBs studied. We also give T_0, the systemic velocity, γ, the radial-velocity semi-amplitude, K, and the reduced χ^2 achieved for the best alias. We also list the period of the Nth best alias and the χ^2 difference between the primary and Nth aliases. For the majority of targets we list the second best alias; however, in the few cases where there are many aliases close in period to the primary alias, we give the first alias for which the period differs from the primary alias by ± 5 per cent. The number of data points used to calculate the orbital period is given in the final column under n.

Object	HMJD (T_0)	Period (d)	γ (km s^{-1})	K (km s^{-1})	χ^2_{reduced}	N	Nth best alias (d)	$\Delta \chi^2$	n
EC00404$-$4429	52894.9418(4)	0.128 34(4)	33.0 $\pm$ 2.9	152.8 $\pm$ 3.4	0.82	2	0.113 50(3)	74	9
EC02200$-$2338	52895.529(4)	0.8022(7)	20.7 $\pm$ 2.3	96.4 $\pm$ 1.4	0.27	2	0.3038(1)	61	10
PG0919+273	53274.29(4)	15.5830(5)	-68.6 ± 0.6	41.5 $\pm$ 0.8	1.23	2	14.9400(5)	43	47
PG0934+186	52376.08(1)	4.05(1)	7.7 $\pm$ 3.2	60.3 $\pm$ 2.4	0.74	2	3.59(1)	22	18
PG0958$-$073	53635.03(2)	3.180 95(7)	90.5 $\pm$ 0.8	27.6 $\pm$ 1.4	2.31	7	2.921 45(5)	29	21
PG1000+408	52920.208(7)	1.049 343(5)	56.6 $\pm$ 3.4	63.5 $\pm$ 3.0	0.73	123	0.705 291(2)	55	20
PG1230+052	53276.431(3)	0.837 177(3)	-43.1 ± 0.7	40.4 $\pm$ 1.2	1.28	70	0.737 931(2)	229	29
EC12408$-$1427	52954.467(5)	0.902 43(1)	-52.2 ± 1.2	58.6 $\pm$ 1.5	0.72	2	9.493(1)	38	29
PG1244+113	53301.61(2)	5.752 11(9)	7.4 $\pm$ 0.8	54.4 $\pm$ 1.4	1.94	2	5.8456(1)	206	51
PG1253+284	53673.77(1)	3.016 34(5)	17.8 $\pm$ 0.6	24.8 $\pm$ 0.9	1.83	2	2.956 92(6)	28	32
EC13332$-$1424	52954.418(3)	0.827 94(1)	-53.2 ± 1.8	104.1 $\pm$ 3.0	0.77	2	0.455 168(3)	33	22
PG1403+316	53293.779(6)	1.738 46(1)	-2.1 ± 0.9	58.5 $\pm$ 1.8	0.88	28	1.638 74(1)	34	16
PG1439$-$013	53629.87(7)	7.2914(5)	-53.7 ± 1.6	50.7 $\pm$ 1.5	1.52	2	7.1452(5)	16	38
PG1452+198	52262.240(4)	0.964 98(4)	-9.1 ± 2.1	86.8 $\pm$ 1.9	0.99	2	0.972 13(4)	2	20
PG1519+640	52391.389(3)	0.539(3)	0.9 $\pm$ 0.8	36.7 $\pm$ 1.2	1.29	2	0.338(2)	68	18
PG1528+104	52394.553(2)	0.331(1)	-49.3 ± 1.0	53.3 $\pm$ 1.6	1.03	2	0.491(2)	33	14
PG1558$-$007	53280.25(4)	10.3495(6)	-71.9 ± 0.7	42.8 $\pm$ 0.8	1.77	2	1.103 666(8)	102	42
PG1648+536	53650.8209(9)	0.610 9107(4)	-69.9 ± 0.9	109.0 $\pm$ 1.3	1.63	37	0.550 0470(5)	202	61
KUV16256+4034	52392.498(2)	0.4776(8)	-90.9 ± 0.9	38.7 $\pm$ 1.2	1.68	2	0.958(2)	64	18
EC20182$-$6534	53276.834(2)	0.598 819(6)	13.5 $\pm$ 1.9	59.7 $\pm$ 3.2	0.84	2	0.585 875(6)	40	25
EC20260$-$4757	53279.37(6)	8.952(2)	56.5 $\pm$ 1.6	57.1 $\pm$ 1.9	2.25	2	0.883 75(2)	22	29
EC20369$-$1804	53279.29(3)	4.5095(4)	7.2 $\pm$ 1.6	51.5 $\pm$ 2.3	0.57	2	0.816 68(1)	20	24
KPD2040+3955	53259.232(3)	1.482 860(4)	-16.4 ± 1.0	94.0 $\pm$ 1.5	3.21	2	1.494 224(4)	37	20
EC21556$-$5552	53660.604(5)	0.8340(7)	31.4 $\pm$ 2.0	65.0 $\pm$ 3.4	1.14	2	0.4545(2)	52	18
KPD2215+5037	53258.172(2)	0.809 146(2)	-7.2 ± 1.0	86.0 $\pm$ 1.5	2.04	147	0.768 551(1)	103	12
EC22202$-$1834	53605.762(4)	0.704 71(5)	-5.5 ± 3.9	118.6 $\pm$ 5.8	0.77	2	0.708 84(5)	5	14
EC22590$-$4819	53278.25(6)	10.359(2)	13.5 $\pm$ 1.1	46.8 $\pm$ 1.8	0.84	2	0.909 70(2)	46	26
PG2331+038	53234.865(3)	1.204 964(3)	-9.5 ± 1.1	93.5 $\pm$ 1.9	2.68	51	0.020 232 962(1)	282	18

this is the criterion by which we consider a system to be solved, since for the practical purpose of comparing the population of sdB stars to theoretical models knowing the periods to within 5 per cent is normally sufficient. In a number of cases, the probability of the orbital period being further than 1 and 5 per cent from our favoured value is the same. This is because all the significant probability lies within a very small range around the best period, with all the significant competition (i.e. next best alias) placed outside the 5 per cent region around the best alias.

We also compute the uncertainty that when added in quadrature to our raw error estimates gives a reduced $\chi^2 = 1$. This systematic uncertainty accounts for sources of errors such as true variability of the star or slit-filling errors. These errors are most probably not correlated with the orbit or the statistical errors determined and thus are added in quadrature. In all cases, we use a minimum value of 2 km s^{-1} corresponding to one-tenth of a pixel which we believe to be a fair estimate of the true limits of our data. These determinations are also given in Table 5. In most cases, the systematic uncertainty does not exceed the minimum value.

4 DISCUSSION

4.1 Effective temperature, surface gravity and helium abundance

We measured the effective temperature, T_{eff}, the surface gravity, log g, and the helium abundance, log (He/H), for 13 of the 28 sdBs

listed in Table 4, and list these measurements in Table 6. Due to the various instrument set-ups we used, we are not able to do this for all the systems, because the data in which the spectral range only encompasses a small number of lines are insufficient to constrain these parameters with any precision. We used the procedure of Saffer et al. (1994) to fit the profiles of the Balmer, the He I and the He II lines present in the spectra by a grid of synthetic spectra. The synthetic spectra obtained from the metal line-blanketed local thermodynamic equilibrium (LTE) model atmospheres of Heber, Reid & Werner (2000) were matched to the data simultaneously. For the two hottest stars the model grid with enhanced metal line blanketing was used, which substantially improved the fits (for details see O'Toole & Heber 2006). Before the fitting was carried out, we convolved the synthetic spectra with a Gaussian function to account for the instrumental profile. KPD2215+5037 was previously analysed with the same set of models in Heber et al. (2002), the results of which are in exact agreement with our finding here.

We plot these results in the T_{eff}/log g plane and find that all but two of the objects lie in the band defined by the zero-age extreme horizontal branch (EHB), the terminal-age EHB and the He main sequence (fig. 2 of Maxted et al. 2001) and are therefore EHB stars. The two exceptions are the two hottest stars, PG0934+186 and PG1244+113, which are sufficiently displaced from the band to be considered post-EHB stars. The effective temperature and gravity of PG1244+113 were determined by Saffer (as reported by Maxted et al. 2001) with a method similar to ours but using a different grid

of synthetic spectra to be $T_{eff} = 33\,800$ K and $\log g = 5.67$, which places it just outside of the EHB band, although the uncertainty on the measurement was such that it could not be positively identified as a post-EHB star. We determine a somewhat higher T_{eff} and lower gravity, which places the star away from the EHB.

We also note that we find EC22133−6446 to be one of the rare helium-rich sdB stars. EC22133−6446 is one of the objects in our survey in which we detect no significant radial-velocity variations.

4.2 Orbital ellipticity

Edelmann et al. (2005) took high-resolution spectra of 15 sdB binaries, and for one-third of these found the orbits to be slightly eccentric with $e \sim 0.03$–0.06. To investigate ellipticity in our binaries we fitted each of our data sets using the Levenburg–Marquardt method (Press 2002) with a model consisting of a sine function and its first harmonic, a reasonable approximation to an elliptical

Figure 1. The radial-velocity curve for each object using the parameters for the best alias given in Table 4, folded on the orbital period. For each object we also plot the residuals to the fit on the same scale, offset by $220\,\mathrm{km\,s^{-1}}$.
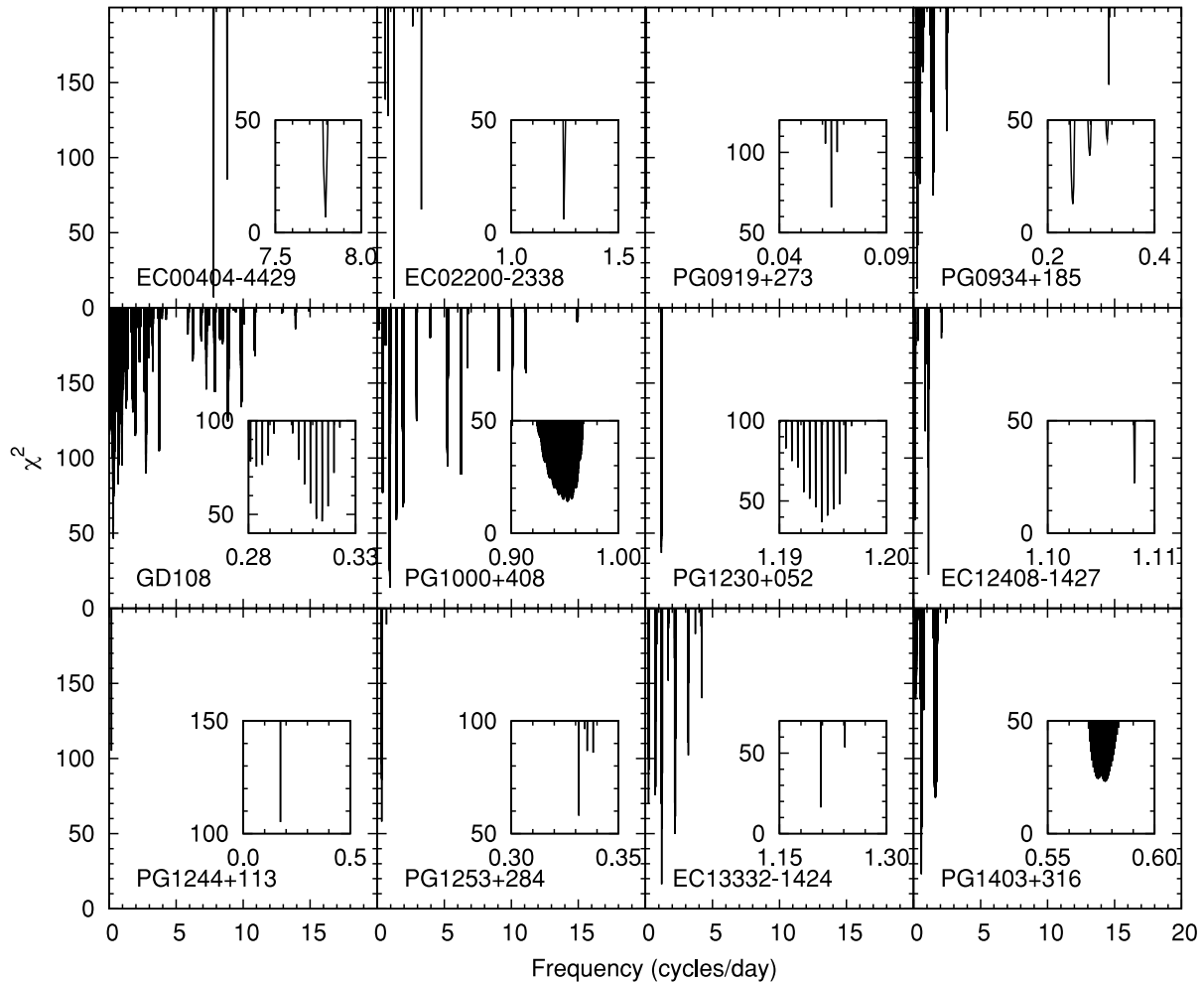
Figure 2. Periodograms for the first 12 objects listed in Table 4. Each panel presents χ^2 versus cycles d^{-1} obtained after the period search was carried out. The frequency with the smallest χ^2 corresponds to the orbital frequency of the system. For clarity, we include an inset showing a blow-up of the region around the orbital frequency.

orbit for small values of e. The eccentricity is determined from the ratio of the amplitudes of the first harmonic to the fundamental. In Table 7 we list the best-fitting value of e for each target and the improvement in χ^2 over a circular orbit. The change in the orbital period determination compared to the values reported in Table 4 is very small (less than 1 per cent in all cases, and much less than this in most). For each target, we computed the F-statistic comparing the elliptical model fit with the circular fit. In all cases, we find that the improvement is not significant at the 95 per cent level. We therefore find that there is no evidence of ellipticity in any of our radial-velocity curves, not even at long periods where departures from circular orbits might be expected.

One important caveat is that our observations were not designed to detect ellipticity in these systems, and it is unlikely that our lower-resolution observations were capable of making significant detections of small eccentricities comparable to those reported by Edelmann et al. (2005). To investigate the limits of our data, we used a Markov chain Monte Carlo (MCMC) algorithm to perturb the elliptical orbit model parameters and compare to our radial-velocity measurements. For each binary, we therefore determined the value of e for which our data are sufficient to give a significant detection. We list the results in Table 7. These are the upper bounds on e, at the 68, 95 and 99 per cent confidence levels. With the

exception of PG0919+273, we find that the upper bound on e at the 95 and 99 per cent levels is much greater than the range reported by Edelmann et al. (2005). We therefore cannot rule out small eccentricities comparable to those reported by Edelmann et al. (2005) in any of these binaries.

4.3 Unsolved systems, non-movers and the binary fraction

In Table 3 we list our radial-velocity measurements for the 108 remaining sdBs which we have observed as a part of this project, but not previously published. In 88 of these systems, we detect no significant radial-velocity variation. These systems are likely to be either single sdBs or binary systems in which the mass function is too low for us to detect radial-velocity variations.

The remaining 20 sdBs do show significant radial-velocity variations, and we consider it likely that most or all of these are binaries. Our current data are not sufficient to distinguish the true orbital period in these systems from various competing aliases, and so these targets are prime candidates for future measurements. We mark these systems in Table 3 with an asterisk. Two systems of particular note are PG1610+519 and PG2317+046. The data we have collected to date suggest that the orbital periods of these systems may be relatively long at 50–70 d.
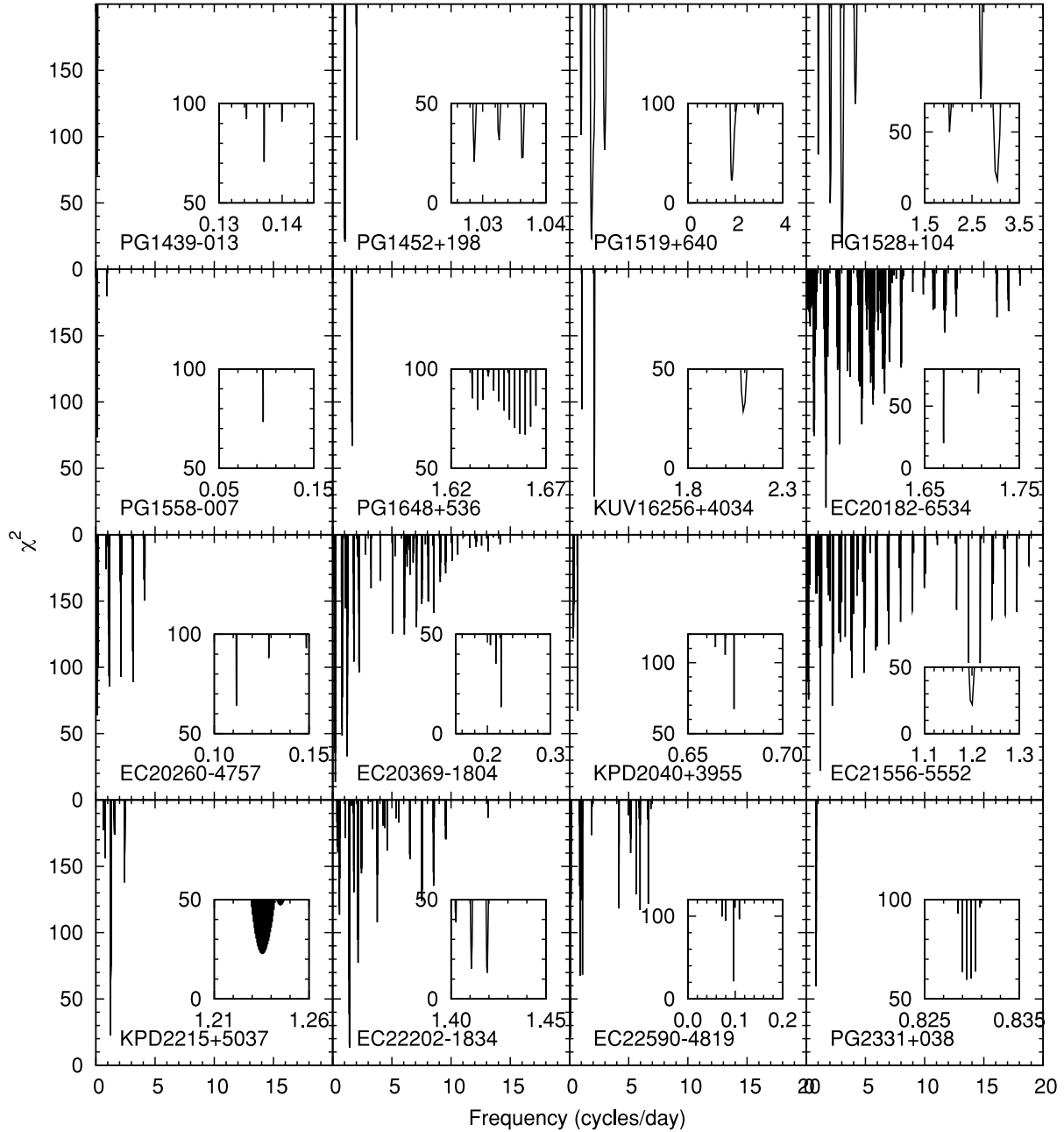
Figure 3. Periodograms as in Fig. 2 for the remaining 16 objects listed in Table 4.

This list of 20 candidate binaries is not exhaustive. As we previously discussed, some fraction of the 'single' sdBs may be long-period systems. There are also a number of sdBs in Table 3 for which we only obtained a small number of measurements and in which there may be large radial-velocity variations which we have missed. There are also some systems in which a small number of measurements suggest a radial-velocity variation which is formally significant, but when we fit them we find that the only possible aliases are very low in amplitude and imply a mass function which is unphysical for an sdB with a stellar companion. We do not mark such systems as binary candidates. However, some authors have discussed the possibility of close substellar companions to sdB stars. One such star in our sample is HD149382. Geier et al. (2009) inferred the presence of a close 8–23 M_J companion to this sdB using

high-resolution radial-velocity measurements, but the more recent data of Jacobs et al. (2011) found no such variation. Our data for this star do show radial-velocity variations which are formally significant. However, we do not believe that these data support the presence of a close companion for two reasons. First, HD149382 has a *V*-band magnitude of 8.9, making it by far the brightest star in our sample (the majority of our targets lie in the $12 > V > 14$ range). For such a bright star slit-filling errors are potentially larger than for faint stars because short exposures lead to larger deviations from the slit centre, and it is possible that we have underestimated these in this case. Secondly, Jacobs et al. (2011) observed a red companion star with a 1-arcsec separation ($\sim$75 au) from the sdB. Given we used a 1-arcsec slit, it is possible that our measurements were contaminated by this distant companion. In general, we believe

Table 5. List of probabilities that the true orbital period of a system lies further than 1 and 5 per cent from our favoured value given in Table 4. Numbers quoted are the logarithms with base 10 of the probabilities. Column 4 gives the value of the systematic uncertainty that has been added in quadrature to the raw error to give a χ^2 that lies above the 2.5 per cent probability in the χ^2 distribution.

Object	1 per cent	5 per cent	Systematic error (km s^{-1})
EC00404−4429	−15.09	−15.09	2
EC02200−2338	−11.35	−11.35	2
PG0919+273	−9.26	−37.27	2
PG0934+186	−3.14	−4.62	2
PG0958−073	−1.42	−3.35	3
PG1000+408	−1.37	−9.57	2
PG1230+052	−17.23	−49.72	2
EC12408−1427	−7.54	−7.54	2
PG1244+113	−25.47	−27.97	4
PG1253+284	−2.70	−14.94	3
EC13332−1424	−5.69	−7.33	2
PG1403+316	−5.06	−5.94	2
PG1439−013	−2.32	−16.55	4
PG1452+198	−14.94	−15.11	2
PG1519+640	−0.98	−3.85	2
PG1528+104	−1.98	−6.83	2
PG1558−007	−18.47	−18.47	3
PG1648+536	−7.10	−35.30	2
KUV16256+4034	−5.74	−13.96	2
EC20182−6534	−8.57	−10.04	2
EC20260−4757	−3.83	−3.83	5
EC20369−1804	−4.40	−4.83	2
KPD2040+3955	−2.75	−7.31	4
EC21556−5552	−8.43	−8.43	2
KPD2215+5037	−6.90	−20.88	2
EC22202−1834	−6.48	−9.21	2
EC22590−4819	−8.82	−8.82	2
PG2331+038	−4.75	−26.72	4

Table 6. T_{eff}, log g and log (He/H). We list only values for the binary systems listed in Table 4 for which our data are sufficient to obtain a good constraint on these parameters.

Name	T_{eff} (K)	log g	log (He/H)
PG0919+273	32 900	5.90	−2.31
PG0934+186	35 800	5.65	−3.00
PG1230+052	27 100	5.47	−2.86
PG1244+113	36 300	5.54	−3.00
PG1403+316	31 200	5.75	−2.42
PG1452+198	29 400	5.75	−2.00
PG1519+640	30 600	5.72	−2.17
PG1528+104	27 200	5.46	−2.52
PG1648+536	31 400	5.62	−4.00
KUV16256+4034	23 100	5.38	−2.99
KPD2040+3955	27 900	5.54	−2.77
KPD2215+5037	29 600	5.64	−2.24
PG2331+038	27 200	5.58	−2.70

that our intermediate dispersion measurements are not sufficient to make convincing claims for any substellar companions to the sdBs in our sample.

As well as these 20 potential binaries and the 28 solved systems in this paper, we previously published 23 binaries in Maxted et al. (2002) and Morales-Rueda et al. (2003b). Additionally, there were

three binaries which were originally on our target list but now have orbital parameters determined by other authors. Our best estimate for the binary fraction in the sdB population is therefore 46 per cent. This is a lower bound for the reasons discussed in the previous paragraph. In addition, some binaries were already known in the Palomar–Green catalogue of sdBs before our project began. Since we may have included these systems in our sample had they not already been solved, our sample is slightly biased *against* binary systems. Including these systems in our binary fraction increases the estimate to 49 per cent.

The initial study of the Palomar–Green sample of sdBs implied a binary fraction of 69 ± 9 per cent (Maxted et al. 2001). However, the sdB binary fraction determined from the ESO Supernovae Type Ia Progenitor surveY (SPY; Napiwotzki et al. 2001) sdB sample was found to contain a binary fraction of 42 per cent (Napiwotzki et al. 2004). Comparing our binary fraction with the SPY result, we note that the SPY authors deliberately chose to exclude known composite spectrum objects from their survey. In Section 4.4 we report 32 composite objects in our target list. When we exclude these objects, our binary fraction increases to 53–56 per cent.

It was thought that the discrepancy between the Maxted et al. (2001) and Napiwotzki et al. (2004) binary fractions could be the result of the different populations surveyed in the two surveys, i.e. SPY looks at stars with white dwarf colours in the thick disc and halo, whereas the Palomar–Green sample consists of targets with sdB colours in the thin disc. Our more extended study of the Palomar–Green sample (and the Edinburgh–Cape sample, which uses similar colour selection cuts) finds a binary fraction which is intermediate between the two earlier figures, and so we believe that the discrepancy is more likely due to low-number statistics, rather than different populations being targeted. Finally, we note that the binary population synthesis of Han et al. (2003) predicted an observable binary frequency of 55 per cent for their best-fitting simulation set (set 2) when selection effects are accounted for, which compares well with our finding.

4.4 The nature of the companion stars

We combine the orbital periods and the radial-velocity semi-amplitudes listed in Table 4 to calculate the mass function, f_{m}, of the system according to the well-known relation

$$f_{\mathrm{m}} = \frac{M_2^3 \sin^3 i}{(M_1 + M_2)^2} = \frac{P K_1^3}{2\pi G},$$

where the subscript '1' refers to the sdB star and '2' to its companion. If we take a canonical mass of 0.48 M$_\odot$ for the sdB star, we can also calculate the minimum mass of its companion, $M_{2\mathrm{min}}$. The values for f_{m} and $M_{2\mathrm{min}}$ obtained in each case are given in Table 8. Additionally, we indicate seven systems for which the companion has been determined to be a white dwarf through the photometric studies of Maxted et al. (2004) or Shimanskii et al. (2008), which showed an absence of reflection effects in these systems, implying a degenerate companion.

Some fraction of the sdB population are composite systems, in which flux excesses at long wavelengths or spectral features indicate the presence of a cool, G–K-type companion. The remaining 'single' sdBs may truly be single stars, or they may have unseen white dwarf or fainter, dM-type companions. Using Two Micron All Sky Survey (2MASS)[1] observations, Stark & Wade (2003) showed that

---

[1] At http://www.ipac.caltech.edu/2mass.

Table 7. For each binary, we list here the best-fitting eccentricity (*e*) and the improvement in χ^2 compared to the circular orbit fit. In all cases, the improvement is not significant at the 95 per cent level. We also give the upper bounds on *e* as determined from our MCMC calculation, at the 68, 95 and 99 per cent confidence levels.

| Name | *e* (best fit) | $\Delta\chi^2$ | Upper bound on *e* | | |
			68 per cent	95 per cent	99 per cent
EC00404−4429	0.06	5.6	0.08	0.11	0.12
EC02200−2338	0.08	0.1	0.25	0.33	0.36
PG0919+273	0.01	0.6	0.03	0.05	0.07
PG0934+186	0.12	5.8	0.16	0.22	0.27
PG0958−073	0.06	0.6	0.12	0.19	0.24
PG1000+408	0.03	0.1	0.16	0.37	0.64
PG1230+052	0.02	0.6	0.05	0.07	0.09
EC12408−1427	0.06	1.3	0.08	0.14	0.17
PG1244+113	0.01	0.2	0.05	0.08	0.10
PG1253+284	0.13	7.5	0.16	0.23	0.27
EC13332−1424	0.03	1.2	0.05	0.07	0.09
PG1403+316	0.12	2.7	0.29	0.55	0.64
PG1439−013	0.13	3.8	0.19	0.32	0.41
PG1452+198	0.05	2.1	0.10	0.16	0.20
PG1519+640	0.13	11.7	0.15	0.20	0.23
PG1528+104	0.12	9.6	0.14	0.18	0.20
PG1558−007	0.06	5.5	0.08	0.11	0.13
PG1648+536	0.05	8.3	0.06	0.08	0.09
KUV16256+4034	0.05	4.9	0.07	0.10	0.12
EC20182−6534	0.06	1.5	0.10	0.16	0.19
EC20260−4757	0.05	1.0	0.11	0.19	0.34
EC20369−1804	0.03	0.2	0.09	0.16	0.21
KPD2040+3955	0.13	11.7	0.15	0.22	0.27
EC21556−5552	0.09	3.5	0.12	0.18	0.21
KPD2215+5037	0.04	3.8	0.05	0.08	0.10
EC22202−1834	0.15	4.5	0.19	0.27	0.33
EC22590−4819	0.03	0.6	0.06	0.10	0.12
PG2331+038	0.05	2.6	0.07	0.11	0.13

the composite and 'single' sdB populations can be distinguished by their $J - K_s$ colour, with the 'single' stars having $J - K_s < +0.05$ and the composites having $J - K_s > +0.05$. In fig. 7 of Stark & Wade (2003) a histogram of the $J - K_s$ colours of all of the sdBs in the 2MASS Second Incremental Data Release showed a clear bimodal distribution. In Fig. 4 we reproduce this histogram for the sdBs in our programme. We plot separately the sdBs which show no radial-velocity variations, the sdBs which are strong binary candidates but without an orbital period determination, and the solved binaries, comprising the 28 systems from this paper and those previously published in Maxted et al. (2002) and Morales-Rueda et al. (2003b). We exclude from this histogram the Kitt Peak–Downes (KPD; Downes 1986) survey objects, since they are close to the Galactic plane and thus potentially significantly reddened.

If we first examine the histogram for the sdBs which do not show radial-velocity variation, we see the same bimodal distribution around a $J - K_s$ value of +0.05 as was found in Stark & Wade (2003). By comparison, the histogram of the solved binaries shows only two systems with $J - K_s > +0.05$: PG1253+284 and PG1558−007. PG1558−007 were identified as a composite system by Allard et al. (1994), but Heber et al. (2002) disputed this identification, attributing the $J - K_s$ colour to interstellar reddening. PG1253+284 was identified as a composite system by Ulla & Thejll (1998), but for this system Heber et al. (2002) determined PG1253+284 (referred to as TON 139 in that paper) to be a triple system via *Hubble Space Telescope* imaging, and concluded that the $J - K_s$ colour in this system is due to the third, distant compo-

nent, and not the companion in the close binary. The third histogram (the potential but unsolved binaries) indicates the presence of a further five composite systems. Aside from the possibility that these are close binaries with a G–K companion, there are three explanations for these measurements. First, some of these composite sdBs may not actually be close binaries: further observations may show that the radial-velocity variations detected to date are not significant. Secondly, some of the $J - K_s$ measurements may be due to a third component, interstellar reddening or a nearby unresolved field star. Thirdly, some of these unsolved binaries may actually be long-period systems, as we noted in Section 4.3.

To investigate this further, we generated mean spectra for all of the objects in our target list and classified them with the aid of synthetic spectra from the grid described in Section 4.1. 25 objects show contamination in their spectra indicative of a cool companion, which would indicate that these are composite systems. We would classify these sdBs as 'double-lined spectroscopic binaries' to distinguish them from the single-lined spectroscopic binaries, the nature of which we identify via radial-velocity variations. There is a strong overlap between the double-lined spectroscopic binaries and the composite systems we identified through 2MASS, with all but five of the 2MASS systems showing a contaminating component in their spectra. We list our candidate composite binaries in Table 9. We exclude PG2059+013 from this table: while the $J - K_s$ colour of this sdB is consistent with it being a composite system, but the Schlegel, Finkbeiner & Davis (1998) dust maps show it to be significantly reddened. This table contains five systems in which we

Table 8. The minimum companion masses $M_{2\,\mathrm{min}}$ and mass functions f_m for the 28 binary systems listed in Table 4, both in units of $\mathrm{M}_\odot$. We also mark 'WD' the seven systems for which the companion star has been determined to be a white dwarf by [a]Shimanskii et al. (2008) or [b]Maxted, Morales-Rueda & Marsh (2004).

Object	$M_{2\,\mathrm{min}}$	f_m	Companion
EC00404−4429	0.316	0.047	
EC02200−2338	0.389	0.074	
PG0919+273	0.480	0.115	
PG0934+186	0.430	0.092	
PG0958−073	0.142	0.007	
PG1000+408	0.250	0.028	WD[a]
PG1230+052	0.132	0.006	WD[b]
EC12408−1427	0.212	0.019	
PG1244+113	0.439	0.096	
PG1253+284	0.123	0.005	
EC13332−1424	0.441	0.097	
PG1403+316	0.280	0.036	
PG1439−013	0.445	0.099	
PG1452+198	0.366	0.065	
PG1519+640	0.100	0.003	WD[b]
PG1528+104	0.127	0.005	WD[b]
PG1558−007	0.412	0.084	
PG1648+536	0.407	0.082	WD[b]
KUV16256+4034	0.101	0.003	WD[b]
EC20182−6534	0.183	0.013	
EC20260−4757	0.589	0.172	
EC20369−1804	0.362	0.064	
KPD2040+3955	0.505	0.128	WD[b]
EC21556−5552	0.234	0.024	
KPD2215+5037	0.333	0.053	
EC22202−1834	0.494	0.122	
EC22590−4819	0.470	0.110	
PG2331+038	0.452	0.102	

Figure 4. Histogram of the $J - K$ colours of the sdBs in our programme, obtained from 2MASS. We plot separately the 100 systems which show no significant radial-velocity variation (top), the 25 systems which are candidate binaries but are currently unsolved (middle) and the solved binaries from this paper, Maxted et al. (2002) and Morales-Rueda et al. (2003b) (bottom).

misidentification had previously been reported for six of these 11 objects. For the other five we give our new classifications, obtained using the same spectral fitting techniques described in Section 4.1.

5 CONCLUSIONS

In this paper we present a large number of radial-velocity measurements of bright sdB stars. The aim of this project was to detect binary systems through variations in these radial-velocity measurements, and hence determine the orbital parameters of those systems. This is a continuation of the work begun in Maxted et al. (2002) and Morales-Rueda et al. (2003b). We presented a total of 28 new binary systems with their parameters, in all cases determining the orbital period to much better than 5 per cent. We determined effective temperatures and surface gravities for 13 of the sdBs in these systems. The parameters are consistent with the sdBs being EHB stars with two exceptions, PG0934+186 and PG1244+113, which we classify as post-EHB stars.

As well as the 28 solved systems we presented measurements for 108 other sdBs. 20 of these show strong signs of binarity, but our data are insufficient as yet to constrain the system parameters. The remaining 100 stars show no significant radial-velocity variations and are likely to be either single sdBs or binary systems in which the orbital period is long enough to push the radial-velocity variations below our detection threshold. Our best estimate for the binary fraction is 46–56 per cent. Finally, we note that none of the binaries we report in this paper shows the near-infrared colours which indicate the presence of a G–K-type companion star. The companion stars in our solved systems are therefore likely either white dwarfs or M dwarfs. There is some evidence for a cool companion in the spectra of 32 of the remaining sdBs, including five which show

believe we detect significant radial-velocity variations, and hence are potentially close binaries.

In summary then, almost all of the systems which we identify as close binaries do not show the presence of a dwarf G–K companion. The companions in these systems are therefore most likely white dwarfs or M dwarfs. The composite systems are almost entirely found in the group of sdBs in which we detected no radial-velocity variations. A G–K companion therefore seems to be indicative of a longer period system: a wide binary in which the sdB has evolved independently of the companion. There are some potential exceptions to this rule: these sdBs are prime candidates for further observation in order to determine if they are indeed binaries, as the data collected to date would suggest, and furthermore if they are close binaries. As we remarked in Section 4.3, two of these candidates (PG1610+519 and PG2317+046) show evidence for binarity, but all of the current aliases suggest a long orbital period, which would be consistent with our composite identification.

4.5 Misclassifications in the literature

Our main source for the construction of our target list was Kilkenny, Heber & Drilling (1988), with the Edinburgh–Cape objects coming from Kilkenny et al. (1997) and private communications. Over the course of our study we discovered a number of sources which have been misidentified as sdB stars in these catalogues, which we have listed in Table 10. At the time of writing they are all still listed as sdBs in the SIMBAD astronomical data base, although the
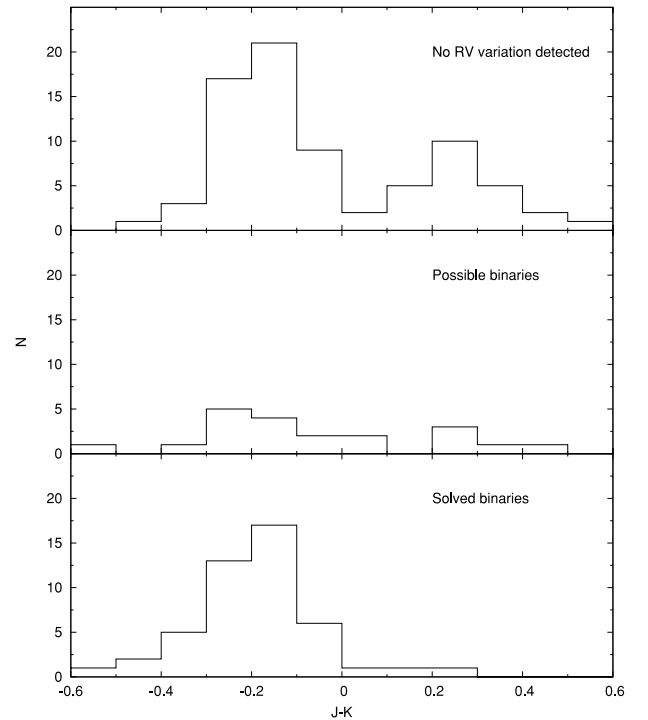
Table 9. sdBs in our sample which show evidence for being composite systems. All of the sdBs we list have 2MASS colours which indicate a cool companion. The majority of these systems are 'double-lined' binaries, in which the inspection of our own spectra shows evidence for a contaminating component. The four systems we list at the end show no such evidence. We also embolden the five objects which show some evidence for binarity through radial-velocity variations.

PG0039+049	EC20117−4014
PB8783	**EC20228−3628**
EC03143−5945	EC20387−1716
EC03238−0710	EC21079−3548
EC04170−3433	PG2110+127
EC04515−3754	PG2118+126
EC05053−2806	EC21373−3727
PG0749+658	PG2148+095
EC09436−0929	PG2226+094
PG1040+234	
EC12473−3046	*2MASS only*
PG1338+611	EC03470−5039
PG1551+256	**PG1526+132**
PG1610+519	EC22133−6446
PG1618+563	**PG2317+046**
PG1701+359	

Table 10. 10 objects in our survey which were misidentified as sdB stars in Kilkenny et al. (1988) or Kilkenny et al. (1997). Six of these objects have previously been reclassified by [a]Gianninas et al. (2010), [b]Saffer et al. (1997) or [c]Ramspeck, Heber & Moehler (2001).

Object	Our classification
KPD 0311+4801	DA, $T_{\rm eff} = 97\,080$ K, $\log g = 6.96$[a]
KUV 04110+1434	MS B-star, $T_{\rm eff} = 13\,000$ K
UVO0653−23	B-star
KPD 0721−0026	B-star, $T_{\rm eff} = 11\,868$ K, $\log g = 3.68$[b]
HD 80836	MS B-star
EC10282−1605	MS B-star, $T_{\rm eff} \sim 16\,000$ K
EC13506−3137	sdO star of unusually low gravity
PG1533+467	MS B-star, $T_{\rm eff} = 18\,100$ K, $\log g = 4.00$[c]
KPD 2022+2033	B-star, $T_{\rm eff} = 16\,752$ K, $\log g = 4.46$[b]
PG2111+023	MS B-star, $T_{\rm eff} = 18\,305$ K, $\log g = 4.5$[b]
PG2301+259	MS B-star, $T_{\rm eff} = 17\,901$ K, $\log g = 4.11$[b]

radial-velocity variations. These are strong candidates for future study.

REFERENCES

Allard F., Wesemael F., Fontaine G., Bergeron P., Lamontagne R., 1994, AJ, 107, 1565
Cumming A., Marcy G. W., Butler R. P., 1999, ApJ, 526, 890
D'Cruz N. L., Dorman B., Rood R. T., O'Connell R. W., 1996, ApJ, 466, 359
Downes R. A., 1986, ApJS, 61, 569
Edelmann H., Heber U., Altmann M., Karl C., Lisker T., 2005, A&A, 442, 1023
Geier S., Edelmann H., Heber U., Morales-Rueda L., 2009, ApJ, 702, L96
Gianninas A., Bergeron P., Dupuis J., Ruiz M. T., 2010, ApJ, 720, 581
Green E. M., Liebert J., Saffer R. A., 2001, in Provencal J. L., Shipman H. L., MacDonald J., Goodchild S., eds, ASP Conf. Ser. Vol. 226, On The Origin of Subdwarf B Stars and Related Metal-Rich Binaries. Astron. Soc. Pac., San Francisco, p. 192
Han Z., Podsiadlowski P., Maxted P. F. L., Marsh T. R., Ivanova N., 2002, MNRAS, 336, 449
Han Z., Podsiadlowski P., Maxted P. F. L., Marsh T. R., 2003, MNRAS, 341, 669
Heber U., 2009, ARA&A, 47, 211
Heber U., Hunger K., Jonas G., Kudritzki R. P., 1984, A&A, 130, 119
Heber U., Reid I. N., Werner K., 2000, A&A, 363, 198
Heber U., Moehler S., Napiwotzki R., Thejll P., Green E. M., 2002, A&A, 383, 938
Iben I., Jr, Livio M., 1993, PASP, 105, 1373
Jacobs V. A. et al., 2011, in Schuh S., Drechsel H., Herber U., AIP Conf. Proc. 1331, Planetary Systems Beyond the Main Sequences. Am. Inst. Phys., Melville, p. 304
Kilkenny D., Heber U., Drilling J. S., 1988, South African Astron. Obser. Circular, 12, 1
Kilkenny D., O'Donoghue D., Koen C., Stobie R. S., Chen A., 1997, MNRAS, 287, 867
Lomb N. R., 1976, Ap&SS, 39, 447
Marsh T. R., 1989, PASP, 101, 1032
Marsh T. R., Dhillon V. S., Duck S. R., 1995, MNRAS, 275, 828
Maxted P. F. L., Marsh T. R., Moran C. K. J., 2000, MNRAS, 319, 305
Maxted P. F. L., Heber U., Marsh T. R., North R. C., 2001, MNRAS, 326, 1391
Maxted P. F. L., Marsh T. R., Heber U., Morales-Rueda L., North R. C., Lawson W. A., 2002, MNRAS, 333, 231
Maxted P. F. L., Morales-Rueda L., Marsh T. R., 2004, Ap&SS, 291, 307
Morales-Rueda L., Marsh T. R., North R. C., Maxted P. F. L., 2003a, in de Martino D., Silvotti R., Solheim J.-E., Kalytis R., eds, NATO ASIB Proc. Vol. 105, White Dwarfs. Kluwer, Dordrecht, p. 57
Morales-Rueda L., Maxted P. F. L., Marsh T. R., North R. C., Heber U., 2003b, MNRAS, 338, 752
Morales-Rueda L., Maxted P. F. L., Marsh T. R., Kilkenny D., O'Donoghue D., 2005, in Koester D., Moehler S., eds, ASP Conf. Ser. Vol. 334, Subdwarf B Binaries from the Edinburgh–Cape Survey. Astron. Soc. Pac., San Francisco, p. 333
Morales-Rueda L., Maxted P. F. L., Marsh T. R., Kilkenny D., O'Donoghue D., 2006, Baltic Astron., 15, 187
Napiwotzki R., Christlieb N., Drechsel H., Hagen H.-J., Herber U., Homeier D., Karl C., Koester D., 2001, Astron. Nachr., 322, 411
Napiwotzki R., Karl C. A., Lisker T., Heber U., Christlieb N., Reimers D., Nelemans G., Homeier D., 2004, Ap&SS, 291, 321
O'Toole S. J., Heber U., 2006, A&A, 452, 579
Press W. H., 2002, Numerical Recipes in C++: The Art of Scientific Computing. Cambridge Univ. Press, Cambridge
Pretorius M. L., Knigge C., Kolb U., 2007, MNRAS, 374, 1495
Ramspeck M., Heber U., Moehler S., 2001, A&A, 378, 907

Saffer R. A., Bergeron P., Koester D., Liebert J., 1994, ApJ, 432, 351
Saffer R. A., Keenan F. P., Hambly N. C., Dufton P. L., Liebert J., 1997, ApJ, 491, 172
Scargle J. D., 1982, ApJ, 263, 835
Schlegel D. J., Finkbeiner D. P., Davis M., 1998, ApJ, 500, 525
Shimanskii V. V., Bikmaev I. F., Borisov N. V., Vlasyuk V. V., Galeev A. I., Sakhibullin N. A., Spiridonova O. I., 2008, Astron. Rep., 52, 729
Stark M. A., Wade R. A., 2003, AJ, 126, 1455
Tutukov A. V., Yungelson L. R., 1981, Nauchnye Inf., 49, 3
Ulla A., Thejll P., 1998, A&AS, 132, 1
Webbink R. F., 1984, ApJ, 277, 355
Yungelson L. R., Tutukov A. V., 2005, Astron. Rep., 49, 871

SUPPORTING INFORMATION

Additional Supporting Information may be found in the online version of this article.

Table 3. Previously unpublished radial velocities for the remaining sdBs in our survey.

Please note: Wiley-Blackwell are not responsible for the content or functionality of any supporting materials supplied by the authors. Any queries (other than missing material) should be directed to the corresponding author for the article.

This paper has been typeset from a T$_{\!E}$X/L^{A}T$_{\!E}$X file prepared by the author.